IEEE Access
Multidisciplinary | Rapid Review | Open Access Journal

Received August 31, 2019, accepted September 17, 2019, date of publication October 7, 2019, date of current version October 30, 2019.

Digital Object Identifier 10.1109/ACCESS.2019.2945978

Spatial Interference Nulling Before RF Frontend for Fully Digital Phased Arrays

ROBIN W. IRAZOQUI, (Student Member, IEEE), AND CALEB J. FULTON, (Senior Member, IEEE)
Advanced Radar Research Center, School of Electrical and Computer Engineering, The University of Oklahoma, Norman, OK 73019, USA
Corresponding author: Robin W. Irazoqui (robinirazoqui@ou.edu)

This work was supported in part by the DARPA under Grant D15AP00090, and in part by the Department of the Navy, Office of Naval Research through the ONR Award under Grant N000141812035.

ABSTRACT Fully digital arrays offer huge advantages in terms of flexibility and performance; however, they may suffer from dynamic range issues when used in the presence of in-band interferers. Higher dynamic range components can be used, but are more costly and power hungry, making the implementation of such technology impractical. This paper presents a way to mitigate those interferers by creating a spatial notch at the RF front-end with an antenna-agnostic circuit placed at the feeding network of the antenna array. This circuit creates a steerable null in the embedded element pattern that mitigates interferers at a specified incoming angle. A full mathematical model and closed form expressions of the behavior of the circuit are obtained and compared to simulated and measured results, where up to a 20 dB null in the embedded element pattern of an 1x8 array is achieved with less than 1.5 dB of insertion loss. Finally, a real case scenario is set up with a desired signal and an interferer, which is initially saturating the receiver. The receiver successfully demodulates the signal after the null is placed in the direction of the interferer.

INDEX TERMS Phased arrays, spatial filters, spatial interference, jammer suppression.

I. INTRODUCTION

The next generation of radar and wireless communication systems should have advanced flexibility, allowing multi-purpose functions and spatial multiplexing while simultaneously reducing cost [1], [2]. Spatial multiplexing for communication systems aims to reduce the exponential increase of spectral cluttering [3], [4] since the demand for mobile data traffic alone is expected to increase 46% annually from 2017 to 2022 [5].

The array architecture that most directly addresses these challenges is that of a fully digital array. Fully digital arrays digitize each element's transmit and receive signals, and beamforming is done in the digital domain. Some serious challenges to successful implementation of digital arrays will be achieving low energy consumption and low cost per antenna element [6], [7]. By independently controlling and digitizing each individual antenna element allows maximum flexibility, but it is achieved at the cost of an increased power consumption. Compared to analog arrays that have only one transceiver, and thus one data stream, digital arrays need larger processing power because of the increase in the number of transceivers and the necessity of handling the high data rates produced [8], [9]. Recent developments in silicon-based integrated circuits have allowed for great technical improvements while reducing cost [7], [10], and enable the option of making fully digital arrays a reality.

Relaxing the dynamic range translates into a reduction of bits needed, and therefore reduces the cost and power consumption [11], [12]. Problems, in terms of dynamic range, arise for fully digital array receivers when strong interferers are present in the environment. The reason such problems do not arise in traditional phased arrays is because they beamform in the analog domain where out-of-beam interferers are mitigated through destructive interference before digitization. In digital arrays, beamforming is done in the digital domain; thus, the receiver array will not benefit from the array factor in the analog domain in the way that traditional analog phased arrays do. As a result of this, higher dynamic range ADCs are needed to resolve a weak signal in presence of a strong interferer [13]. Strong interferers can drive the active components into the non-linear region of operation, or even

The associate editor coordinating the review of this manuscript and approving it for publication was Zhu Han.

saturation, consequently significantly degrading the quality of the desired signal.

Research has been done to improve the dynamic range of a receiver in the presence of RF interferers through digital nonlinear equalization (NLEQ). Such interferers may produce higher-order intermodulation products in the receiver chain, corrupting the desired signal [14], [15]. This technique linearizes the signal and conditions it for further processing to help mitigate these distortions. NLEQ techniques have been proven to be effective only under relatively ''weak'' nonlinearities, but better solutions are needed to solve this issue for strong interferers.

Adaptive digital beamforming (ADBF) digitally cancels the interferers that are present in the beamformed signal, but under the assumption that the individual receivers have not been compressed; otherwise, spatial correlation can create distortion products that are in the direction of the signal of interest [2].

Ideally, this spatial and spectral interference mitigation would occur at the antenna element itself, before any active electronics are involved at all. Research in the integrated circuits (IC) domain has investigated using active electronics in the RF front-end and baseband regimes. For example, a full four-element integrated MIMO receiver array with 8 dB spatial interference mitigation at the RF front-end by using a spatial notch filter (SNF), and another 24 dB of cancellation at baseband before digitization was developed in [7], using a technique known as Feed-forward Spatial-Notch Cancellation (FFSNC). A total of 51 dB mitigation with moderate impact in the noise figure of $3.4 - 5.8$ dB and the ability to create multiple notches is demonstrated in [16]. This approach implies designing a fully integrated receiver resulting in lack of flexibility because the RF system must use only that specific receiver architecture in order to have a front-end spatial filter. Other approaches, such as having a beamformer integrated in the LNA were presented in [17]. The beamformer selects the interferer and feeds it deconstructively into the amplifying stage of the LNA to cancel out the interfering signal. Mitigation of up to 20 dB of attenuation was achieved with a simulated noise figure of 6.7 dB, thereby impacting the sensitivity of the receiver. Both approaches use complementary metal-oxide-semiconductor (CMOS) technology that compromises the power handling limitation when strong interferers are present. These CMOS RF front-end architectures suffer from a trade-off between noise figure and power handling. This trade-off is caused because high gain is needed at the RF front-end to reduce the noise figure, but due to low supply voltages used in current CMOS processes, even a 0 dBm interferer will can cause the amplification stage to clip and will result in a dynamic range limitation [18]. Another way to handle spatial interference is by using the Butler matrix, but they suffer from scalability problems for large arrays due to size.

This paper introduces a Spatial Interference Mitigation Circuit (SIMC) that is able to mitigate interferers at the RF front-end before they enter the receiver by creating a steerable null in the antenna's embedded element pattern. This work mathematically proves that this technique is antenna agnostic for large arrays. It also means that it can be placed at any stage of the RF layer, but this paper focuses on placing the circuitry at the feeding network. This work proposes to interconnect the antenna elements placed in the array by using passive components. The only active components needed are phase shifters to steer the null. Potentially one of the most attractive features of this technique is that it is antenna agnostic and therefore can be applied to practically any array.

In [19], the concept of the SIMC was presented and applied to a practical scenario. The SIMC was later used with a focus on digital post-processing in [20] to increase the overall dynamic range of the system. In this paper, the authors build on the previous work and present the fundamental mathematical theory and modelling of the SIMC. A new, high efficiency SIMC is designed and measured, showing a lower insertion loss (IL) and an increase in the nulling selectivity. This improvement leads to developing a system-level linear analysis. This paper also provides measured embedded element patters of an 1x8 array and provides further details on a real-world scenario.

In section II a complete mathematical model is introduced, describing the behaviour of this circuit when placed in an infinite array environment. A closed form expression is obtained to determine the parameters needed in that circuit to place a null at a specified scan angle. In section III the mathematical model is validated with simulated and measured embedded element patterns obtained from the anechoic chamber. Finally, section IV presented a 'real case scenario' where an interferer is saturating the receiver and prevents it from receiving a QPSK signal at broadside. The signal is demodulated once the null is placed in the direction of the interferer.

II. SPATIAL INTERFERENCE NULLING TECHNIQUE

The final goal of this research is to apply this technique to large arrays. Therefore, an infinite array approach has been used to derive the mathematical model to describe a front-end SIMC and predict where the nulls are placed in the spatial domain. The performance of a large finite array can be precisely modeled using infinite array theory and it assumes that all antennas have equal embedded element patterns, the edge effects are negligible, and mutual coupling combined with the self-impedance is embedded in one variable called the active reflection coefficient. The mutual coupling is treated through the use of Floquet ports and master/slave boundary conditions [21]. The traditional way to describe an infinite array environment is by using the definition of a unit cell [21]. A unit cell defines the electromagnetic properties of a single radiating element when it is placed equidistant from copies of itself that form an infinite array. The authors of [21] prove that mutual coupling, along with self impedance, leads to the concept of an active impedance. This method is widely used to design large antenna arrays.

Fig. 1 illustrates a unit cell placed in an infinite linear array in which each element is composed of an antenna, a SIMC and the receiver or RF front-end port. The only difference between adjacent unit cells is a progressive phase shift ϕ of all signals and fields. The equivalent schematic proposed is shown in Fig. 1, where the antenna feeds the received signal directly into the SIMC. This circuit is composed of a quadrature hybrid (QH) and an undefined two-port network, for which properties need to be found in order to generate a null for a certain angle of incidence. This SIMC is placed in a layer that goes between the radiating element and the transceiver's front-end. In Fig. 1 the quadrature hybrid interconnects the antenna's port (Port 2) with the transceiver's front-end (Port 1). Since one of the properties of the quadrature hybrid is to split its power, the resulting wave at Port 3 is used to feed the cancelling signal into its adjacent element through the two-port network. This two-port network modifies the cancelling wave in gain and phase in such a way that it adds destructively into its adjacent element through Port 4 in order to achieve a null for a desired scan angle. The SoI coming from different angles will go into the adjacent element through the two-port network and will feed constructively. The SIMC's equivalent physical structure is shown in the SIMC layer of Fig. 2 where the circuitry is connected directly to the via-fed patch antenna shown as radiating layer.

Scattering Matrix analysis is used to describe the mathematical model, where a QH S-parameter matrix is nominally given as

$$\left|S_{quadrature\ hybrid}\right| = \frac{1}{\sqrt{2}}\begin{vmatrix} 0 & -j & -1 & 0 \\ -j & 0 & 0 & -1 \\ -1 & 0 & 0 & -j \\ 0 & -1 & -j & 0 \end{vmatrix} \tag{1}$$

The S-parameters for an unknown two-port network can be expressed as

$$\left|S_a\right| = \begin{vmatrix} S_{11a} & S_{12a} \\ S_{21a} & S_{22a} \end{vmatrix} \tag{2}$$

where $S_{11a} = S_{22a} = 0$ because perfect matching is assumed. For simplicity, the initial assumption is that the two port network is symmetric, therefore $S_{12a} = S_{21a} = G \cdot e^{-j\theta_2}$. The gain and phase of this two-port network is what needs to be found in order to get a null for a certain scan angle. Under these assumptions, and denoting the incident and reflected voltages with + and − subscripts, respectively, expressions like the following can be obtained for when operating in receive mode:

$$V_1^- = V_2^+ S_{12} + V_3^+ S_{13} \tag{3}$$
$$V_3^+ = V_{1a}^- \tag{4}$$
$$V_4^- = V_2^+ S_{42} + V_3^+ S_{43} \tag{5}$$
$$V_{1a}^- = V_{1a}^+ S_{11a} + V_{2a}^+ S_{12a} \tag{6}$$
$$V_{2a}^+ = V_4^- e^{-j\phi} \tag{7}$$

ϕ is the progressive phase shift produced at each antenna element for an incoming wave at an angle θ away from broadside. The relationship between these two values for a linear array can be expressed as

$$\phi = kdsin(\theta) \tag{8}$$

where k is the wave number and d is the distance between elements. V_1^- is the voltage going into the transceiver, as shown in Fig. 1, and a closed form expression for V_1^- can be calculated for an incoming wave, exciting port 2 creating an input voltage V_2^+, resulting in

$$V_1^- = \left[S_{12} + S_{13}\frac{S_{12a}S_{42}e^{-j\phi}}{1 - S_{12a}S_{43}e^{-j\phi}}\right]V_2^+ \tag{9}$$

From the above expression it is clear that the voltage going into the receiver (V_1^-) is dependent on the properties of the QH, the S-parameters of the two-port network, and the progressive phase shift throughout the array due to a plane-wave arriving at an incoming angle. V_2^+ is the input signal to the unit cell from the antenna element when excited by a plane wave coming in from an angle of θ, and takes into account effects from radiation and coupling. The goal is for V_1^- of (9) to be zero for a certain θ. Once θ is converted to the progressive phase shift using (8), S_{12a} can be extracted by solving $V_1^- = 0$ in (9). A closed form expression is obtained for S_{12a} that can be written as

$$S_{12a} = \frac{S_{12}}{S_{12}S_{43} - S_{13}S_{42}}e^{j\phi} \tag{10}$$

where it can be observed that S_{12a} is not a function of V_2^+. This means that the effects of mutual coupling and self impedance do not affect the magnitude or phase required from

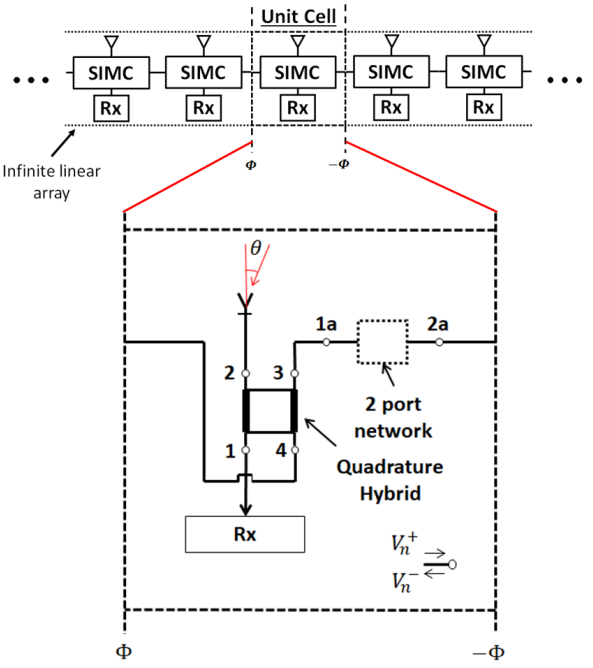

FIGURE 1. Illustration of a unit cell extracted from an infinite array. The proposed structure of the SIMC placed in a unit cell is shown below.

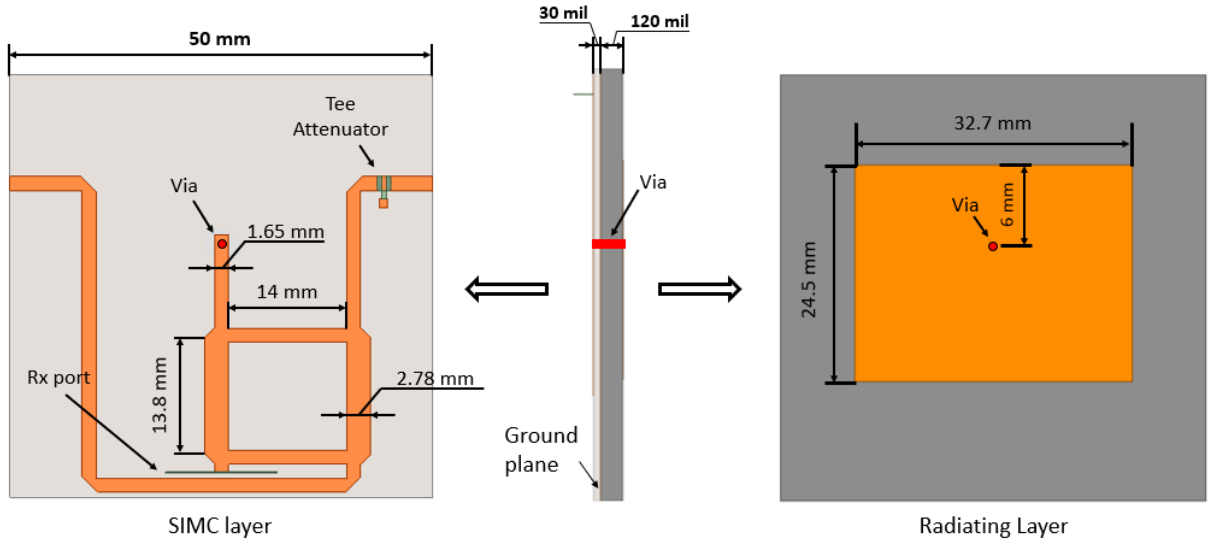

FIGURE 2. 3D model of the simulated structure showing the stacked layers. The left figure illustrated the top layer where the SIMC is placed, the middle figure shows how the structure is stacked, and the bottom layer is shown at the right where the patch antenna is placed conforming the radiating layer.

the two-port network. It can be concluded from this mathematical result that the SIMC is antenna agnostic and can be placed anywhere in the RF front-end. If strong interferers are the main concern, the SIMC should be placed immediately after the antenna. However, other applications might be of interest, for example, a useful placement of the SIMC would be after the receiver's LNA to improve the noise figure, so long as the LNA can handle the dominant interferer.

In order to create the null for a certain θ, ϕ needs to be set using (8) and the gain and phase can be obtained from (10). This equations shows that the magnitude of S_{12a} will remain constant for different null placements along θ and it is only dependent on the S-parameters of the QH. The gain will be $|S_{12a}| = 1/\sqrt{2}$ (or a 3 dB attenuator as shown in Fig. 2) for an ideal equal split QH, which implies that this circuit is passive. Once the S_{12a} is calculated from (10), the response of the of the signal going into the receiver versus the incident angle can be calculated by using the expression derived in (9).

A. SIMC UNIT CELL SIMULATED RESULTS

The easiest way to verify that a null is accurately positioned for a certain incoming wave is by using a full-wave electromagnetic simulator (HFSS). An infinite array approach was used in HFSS to verify the results obtained with the mathematical model, because they both use the unit cell representation. A $\lambda/2$ size unit cell was designed, emulating a planar infinite array approach using Floquet ports and master/slave boundaries. The SIMC is designed on a 3D structure with a Rogers 4350B dielectric, chosen because of its low cost and low loss. The thickness of the Rogers 4350B dielectric is 30 mils and it operates at 2.75 GHz. The full structure (shown in Fig. 2) uses three layers; the top layer has the SIMC, the middle layer is composed of a ground plane, and the bottom layer is composed of the radiating element, initially a patch antenna. However, the patch antenna is replaced with a port to simulate the performance of the spatial interference mitigation network independently of the performance of the antenna. The simulated S_{12a} is composed of a Tee-network to obtain the required IL, and a variable length transmission line to set the correct phase.

The mathematical and simulated results can now be compared, as shown in Fig. 3, where a close agreement is seen between the mathematical model and the simulated results. The figure shows the response of the SIMC for three different nulling angles (-43, -20 and 5 degrees). The stop-angle is defined as the angle that has the maximum rejection out of all angles of the spatial response. At the stop-angle, the signal gets successfully deconstructed for the incident angle. At the pass-angle, the signal from its adjacent element adds constructively with the signal produced by the excitation and contributing to a reduced overall IL.

Fig. 3 shows an achievement of nulls that provide up to 25 dB of mitigation for the simulated results. The fractional bandwidth (FBW) of the null at 3 dB is 7.5 % and at a depth of 10 dB the FBW is 2.5 %. The mathematical model allows the extraction of optimal attenuation values because it takes into account the loss of the traces, as well as slight imbalances in a real QH. Optimal attenuation values translate into a deeper null. Due to loss and component imperfections, the attenuation that gave the best performance was found to be $S_{12a} = 2.81$ dB instead of the 3 dB of that derived in the ideal case.

B. PERFORMANCE OPTIMIZATION AND SYSTEM LEVEL ANALYSIS

The mathematical model proves that it is theoretically possible to place a null in the spatial domain and mitigate the interferer before it reaches the RF front-end. It would be

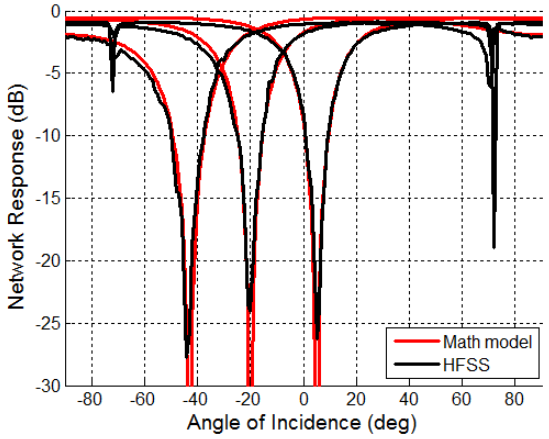

FIGURE 3. Comparison between the mathematical model (red) and HFSS simulations (black) of the signal going into the receiver versus scan angle.

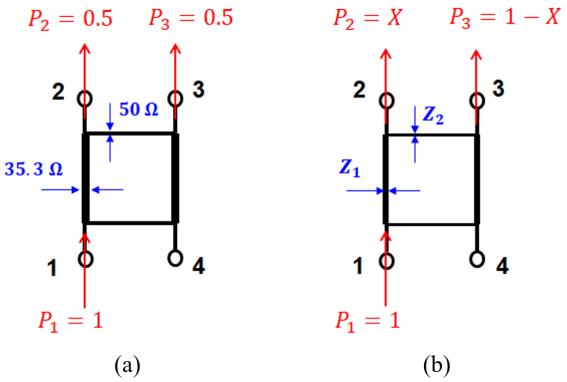

FIGURE 4. Illustration of a schematic of (a) an equal split QH and (b) an unequal split QH.

highly beneficial if the SIMC could provide a higher level of flexibility, such as being able to change the null width and manipulate the overall IL. In the previous section, a regular equal power split QH was assumed. This QH equally divides the power passing through port 1 between ports 2 and 3 as shown in Fig. 4a. The response from (9) is a function of the S-parameters of the QH, and V_1^- can be modified when using unequal split QHs.

Knowing that a QH is a symmetrical passive device, the S-parameter matrix can be rewritten as

$$\left|S_{quadrature\ hybrid}\right| = \frac{1}{\sqrt{2}} \begin{vmatrix} 0 & S_{12} & S_{13} & 0 \\ S_{12} & 0 & 0 & S_{24} \\ S_{13} & 0 & 0 & S_{34} \\ 0 & S_{24} & S_{34} & 0 \end{vmatrix} \tag{11}$$

The goal is to see how the performance of the SIMC varies when different power distributions flow through the QH. S_{12} is the voltage going from port 1 to 2 and is going to be defined as the dependent variable set by the user. Assuming that the QH is lossless, then from (11)

$$|S_{13}|^2 = 1 - |S_{12}|^2 \tag{12}$$

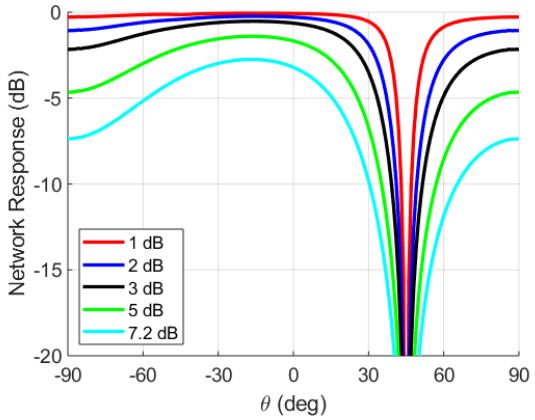

FIGURE 5. Performance of the SIMC when using different unequal split QHs S_{12}/S_{13}.

When substituting the previous equation in the second and third row of (11) it results in

$$|S_{24}|^2 = 1 - |S_{12}|^2 = |S_{13}|^2 \tag{13}$$

$$|S_{34}|^2 = |S_{12}|^2 \tag{14}$$

The new S-parameters are only modified in magnitude. The electrical length between ports remain unchanged at $\lambda/4$ and maintain the same phase difference between ports as occurs in the equal split design. The new S-parameter values defining the unequal split QH are a function of S_{12} and are theoretically realizable because these new expressions for S_{13}, S_{24} and S_{34} comply with the unitary matrix. Simulations were run when substituting the new S-parameters in the closed-form expression from (9). The results are shown in Fig. 5. A more selective null and less overall IL is achieved when increasing the ratio of $|S_{12}|/|S_{13}|$. The results shown in Fig. 5 are very beneficial because the improvement of the IL of the SIMC is related to the width of the null. Ideally however, they would be uncorrelated.

Fig. 6 shows the spatial response of the power of a signal that flows through the whole system when the null is placed at 45° for a received signal of 0 dB at port 2 (P2). Fig. 6a shows the power in relation to the angle of incidence when the QH has an equal split ($S_{12} = 3$ dB). A more optimized case is shown in Fig. 6b for an unequal split QH with $S_{12} = 1$ dB. When the system is in receive mode, a plane wave will excite P2 of the QH with a normalized power of 0 dB after de-embedding the active reflection coefficient. As expected for the pass-angle (any angle besides 45°), most of the power will flow directly into port 1 (P1) which is the node connected to the RF front-end. The power going into the cancelling feeding path, represented as port 3 (P3) and port 4 (P4), will be minimal for the pass angles. When the incident wave is at the incoming angle of the null placement, the power going into P1 tends to approximate to 0 ($-\infty$ in dB). Since the system is lossless all the power is redirected into the cancelling feeding path, P3 and P4. That means that there is a negative impact when decreasing the IL of the SIMC. That

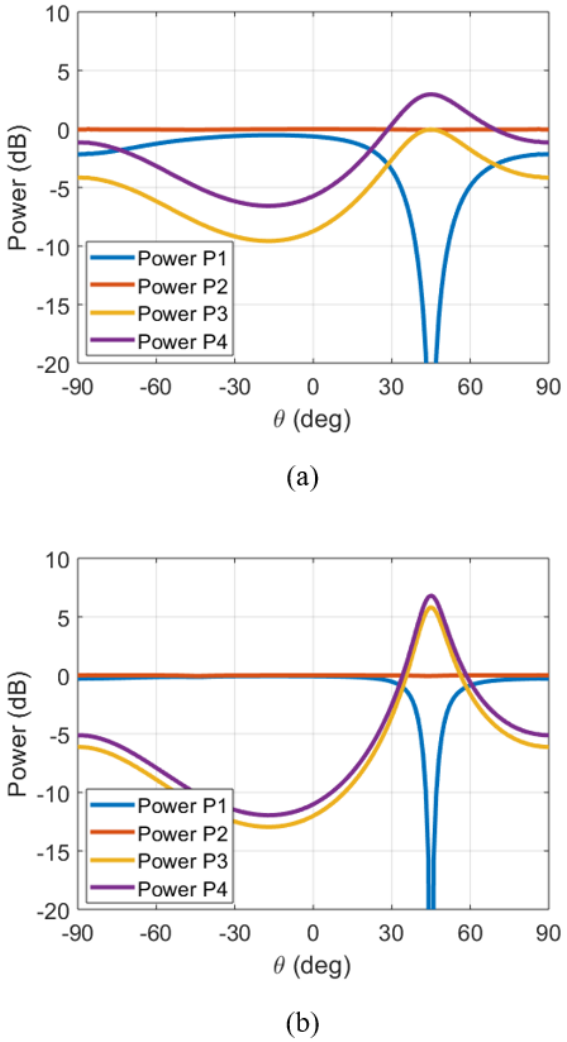

FIGURE 6. An illustration of the power flow into (ports 2 and 3) and out of (ports 1 and 4) the QH vs. angle for the SIMC where (a) uses a equal split quadrature hybrid and (b) an equal split quadrature hybrid with $S_{12} = 1$ *dB*.

trade-off is shown in Fig. 6b when the cancelling signal flows with higher power through the general two-port network after increasing $|S_{12}|$. That increase goes from 3 dB for an equal case to 6.8 dB for the $P_{12} = 1$ dB case, as shown in Fig. 6. This might be a concern because in order to get real-time null-steerability, the general two-port network will most likely be an active or semi-active component. A higher power flowing through an active component can compromise its linearity, creating harmonics and decreasing the system's dynamic range. The reader might observe in Fig. 6 that the normalized power exceeds 1 (0 dB) this phenomenon is explained in more detail in the next section.

It is mathematically proven that the IL loss can be decreased and the null can be narrowed, allowing for a lower noise figure and a more efficient interferer free scanning volume. When changing the power distribution of the QH, the properties of the general two-port network also need to be changed. From (10) it can be seen that the IL of that two-port network is only a function of the S-parameters of the QH. When (13) and (14) are substituted in (10) and the magnitude is taken, it is found that

$$|S_{12a}| = |S_{12}|. \tag{15}$$

This result shows that the IL of the two-port network needs to be the same as the S_{12} of the QH. It is also shown that there is a relationship between the IL of the two-port network (or QH) and the spatial response.

The unequal power split is obtained by changing the characteristic impedances of the lines. The impedances of the lines (Z_1 and Z_2) defining the QH shown in Fig. 4b can be found using even and odd mode analysis. It is beneficial to calculate the impedances as a function of gain defined as V_{P2}/V_{P3} because the result can then be related directly to S_{12} of the QH. Then Z_1 can be expressed as

$$Z_1 = \sqrt{\frac{Z_0^2 Z_2^2}{Z_2^2 - Z_0^2}} \tag{16}$$

Z_1 ensures that the quadrature is matched to the characteristic impedance (Z_0) of the system. Z_2 defines the power split between P2 and P3 and it equates to

$$Z_2 = Z_0 \sqrt{\frac{G^2}{1 - G^2}} \tag{17}$$

This infinite array mathematical analysis and simulations of large arrays show a promising way to optimize the SIMC for more selective nulls and a reduced IL; however, a finite array is needed in order to build a system and measure its performance.

III. 1X8 FINITE ARRAY DEMONSTRATOR

The mathematical model derived above for a unit cell representing an infinite array approach closely agrees with simulated results. However, a finite array is needed to prove that this structure works in a real environment. In this section, measurements are taken and compared to simulated results. Since the mathematical model and the simulated model closely agree for the infinite array case, a close agreement between measurements and simulated results, for a finite array case, would further validate the mathematical model. With the use of HFSS, the authors concluded that a 1x8 array would be an excellent size array to show the effects of the SIMC, due to low requirements of computational resources, while still being big enough for the spatial response to converge towards the results found for the infinite array (as explained in the next subsection). The infinite array response is of interest because it serves as the reference of the null's magnitude. First, the array using the SIMC with an equal split QH is simulated and verified that it is performing as expected. That same array is later fabricated and tested. Finally, a SIMC that uses electronically configurable phase shifters for real-time null steering is designed and fabricated, and its simulated results are compared to the measurements.

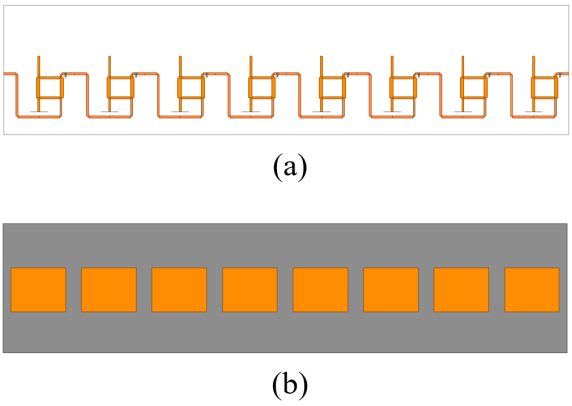

FIGURE 7. An illustration of the 3D structure of the simulated model where (a) is the top layer and is connected with vias to (b) the radiating layer.

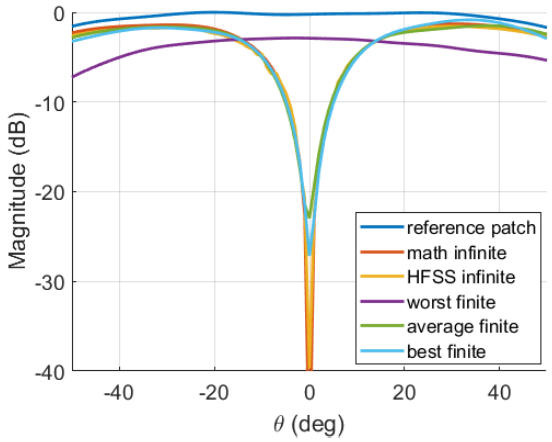

FIGURE 8. Comparison between a patch antenna without SIMC, the mathematical model, HFSS infinite array approach and HFSS worst, average and best performing element of an array with null scanned to broadside.

A. 1×8 SIMC ARRAY SIMULATION USING EQUAL SPLIT QUADRATURE HYBRIDS

The 1x8 array layout was completed by duplicating eight times the unit cell from Fig. 2, and results in the structure shown in Fig. 7. Since it is a finite array, the edge elements are terminated using 50 Ω loads. In particular, the terminations include port 3 of element 1 and port 4 of the element 8. These terminations are the same as for the measured array shown in the block diagram of Fig. 9. The dielectric used for the radiating layer is a 125−mil thick Duroid 5880.

The results shown in Fig. 8 reflect the performance of the worst, average, and best finite array responses of a simulated 1x8 array, and are compared to the spatial response of the infinite array. The mathematical model accurately predicts the performance most elements. The worst performing element will always be the first element of the array because it has no signal from the adjacent element to provide destructive interference for the null or constructive interference for the desired scan angles. After the first element, the cancelling

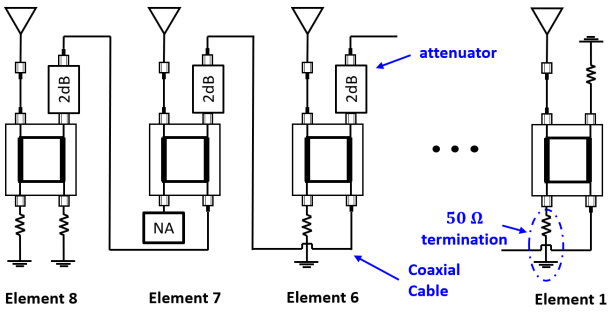

FIGURE 9. Illustration of the schematic of the measurement setup of the 1x8 array with SIMC and coaxial cables where the embedded element pattern of the 7th element is measured.

signal starts to increase in amplitude as it progresses through the elements of the array until it approximates the amplitude of the infinite array response. After taking multiple measurements, it was found that the 3rd or 4th element and onwards will show a spatial response that approximates the infinite array response. The authors believe that having poor performance of the first few elements will be negligible when this technique is applied in large arrays. To further support this idea, it should be noted that dummy elements are frequently placed on the edges of large arrays [22] to improve thier active match and sidelobe levels anyway.

The reduced performance of the first elements helps explain why some of the power flows in Fig. 6 (for the infinite array case) exceed unity. The QH takes the power of the first few elements and feeds it into the cancelling path of subsequent elements until the amplitudes of the signals approach the amplitude derived for the infinite array case. Therefore, in a finite array, the fact that the power of the cancelling signal is more than 0 dB when the input signal is 0 dB, is possible by ''sacrificing'' the performance of the first elements. As is typical of all finite arrays, accurate prediction of embedded behavior of the first few elements for a SIMC-enhanced array would require a more detailed analysis of the specific edge effects in play.

B. 1×8 EQUAL SPLIT QUADRATURE HYBRID SIMC ARRAY MEASUREMENTS

The array was fabricated after verifying that a finite array would reasonably capture large or infinite array behavior. Due to panel size constraints in the fabrication process, the 1×8 element radiating layer was build on two panels containing 4 patch antennae each. The SIMC layer was composed of 8 separate QH that were interconnected with coaxial cables as shown in Fig. 9. When considering losses and the SIMC use of an equal split QH, the resulting IL needed for S_{12a} was 2.8 dB. Coaxial cables and female-to-male connectors were used to provide phase shifting for null steering, and had a measured IL of about 0.8 dB; therefore, a 2 dB attenuator was used (adding to a total value of 2.8 dB, approximately the same as the optimized solution shown in Figure 3). The phase shifting for θ_2 was created by using a coaxial cable and a

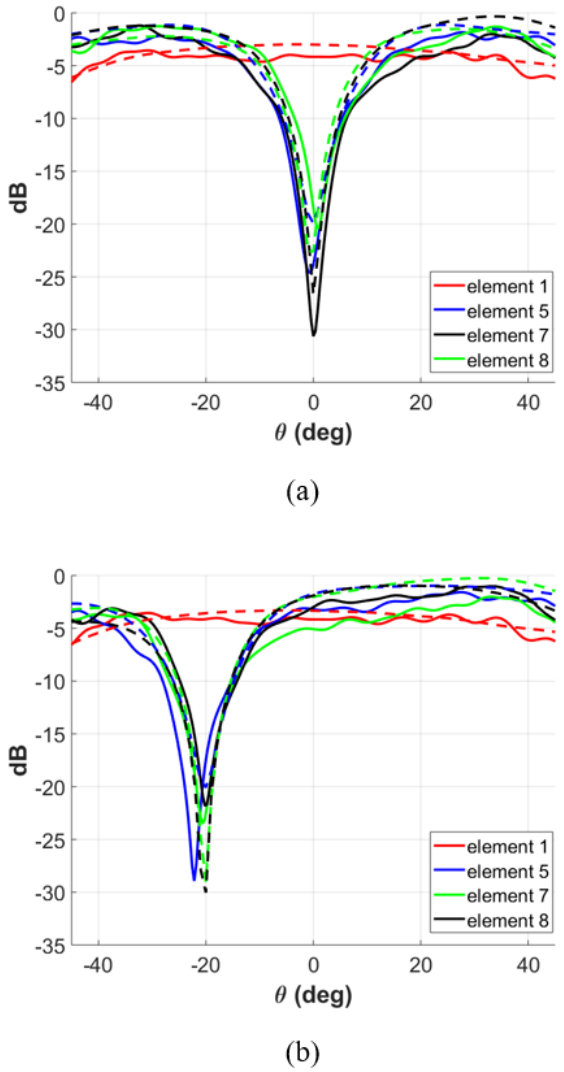

FIGURE 10. Measured vs simulated embedded element patterns for the equal split QH case for two different null placements. The solid lines are measured results and dashed lines are simulated results. Measured results are normalized using measurements of the same array with the SIMC removed.

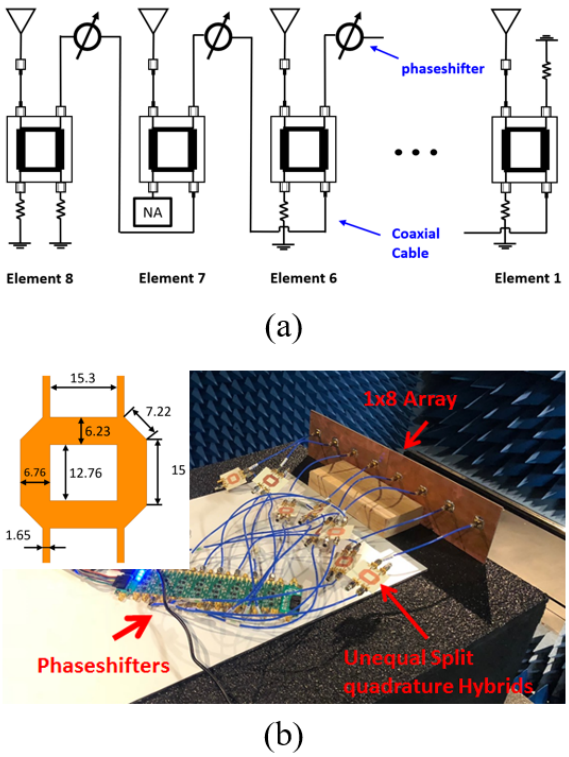

FIGURE 11. Illustration of the 1x8 array with SIMC using phase shifters, (a) shows the schematic of the measurement setup where the embedded element pattern of the 7th element is measured, (b) is the illustration of the whole system in the anechoic chamber with an amplification of the unequal QH and its dimensions.

female-to-male adapter, which add an extra 70° of delay each at 2.75 GHz, replicating a tunable electrical length. Those extra delays will change the phase of the cancelling signal feeding into the adjacent element and changes the location of the nulls. Two different null placements where obtained using: none and 1 female-to-male connectors. Knowing the total delay of the line θ_2, the nulls were predicted to occur at 0° and −20° according to the mathematical model in (9). The simulated results of the finite array are compared to the mathematical model in Fig. 8 where the worst finite was the response of the 1st element, and the 7th element was the one that showed the best response. The 5th element shows that the array is already operating near its peak performance. The 8th element is shown because it was the element used in the next section.

The SIMC spatial performance using the equal split QH is shown in Fig. 10 and illustrates measured vs simulated embedded element patterns for the 1,5,7 and 8th element of the 1x8 array with nulls at 0° and −20°. As previously discussed, the first element has a reduced performance, but the other elements have an IL of less than 1 dB (considering that the roll-off of the antenna pattern is embedded in the result too). The average IL of all the embedded element patterns is 1.16 dB at best. Nulls of 15 dB are usually achieved after the 4th element.

C. 1X8 SIMC ARRAY PHASE SHIFTER FOR REAL-TIME STEERING

The second SIMC was designed to accommodate an electronically steerable null implemented with phase shifters. Those phase shifter boards were pre-programmed and readily available to the authors of this research. The drawback was that the IL of those phase shifters oscillated between 7.2 and 7.7 dB as a function of angle. That meant that an unequal split QH was designed and fabricated as shown in Fig. 11b, changing the line impedances to $Z_1 = 18.79\ \Omega$ and $Z_2 = 20.28\ \Omega$ according to (16) and (17). The unequal power split was designed consequently with the results obtained from (9) to compensate for the high IL. *The consequence was an increase of the overall IL of the system; however, it served as a proof of concept for real-time electronic null steering without ready access to low-loss (< 2 dB) phase shifters*. The blok diagram of the experimental setup is shown in 11a, where individual

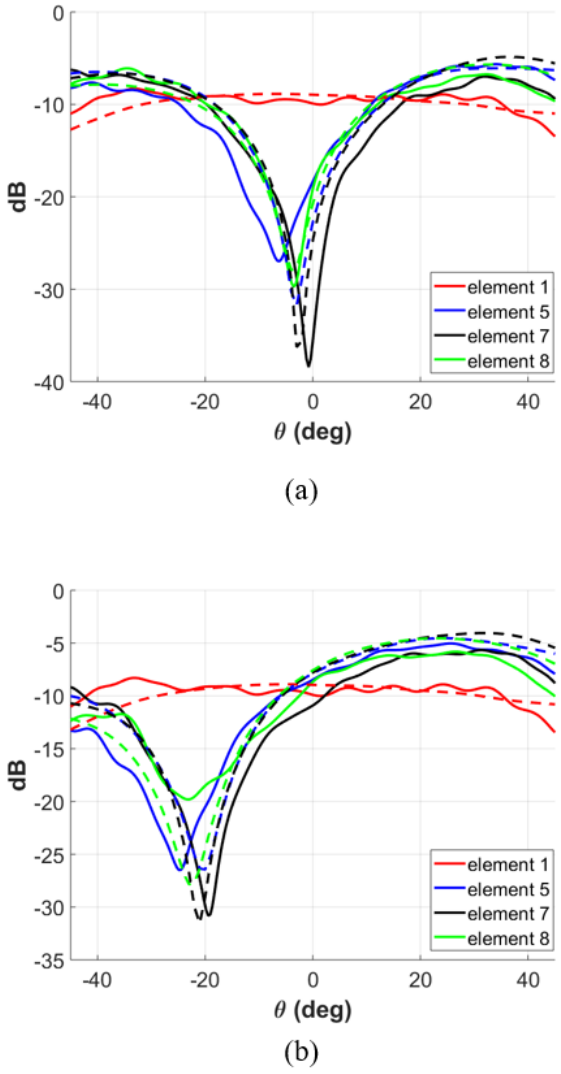

FIGURE 12. Measured vs simulated embedded element patterns for the unequal split QH case (with phase shifters) two different null placements. The solid lines are measured results and dashed lines are simulated results.

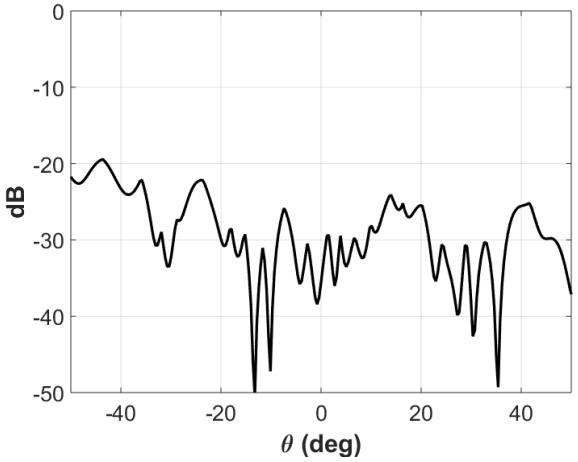

FIGURE 13. Illustration showing the measured null depth of the 7th element versus angle when sweeping the null.

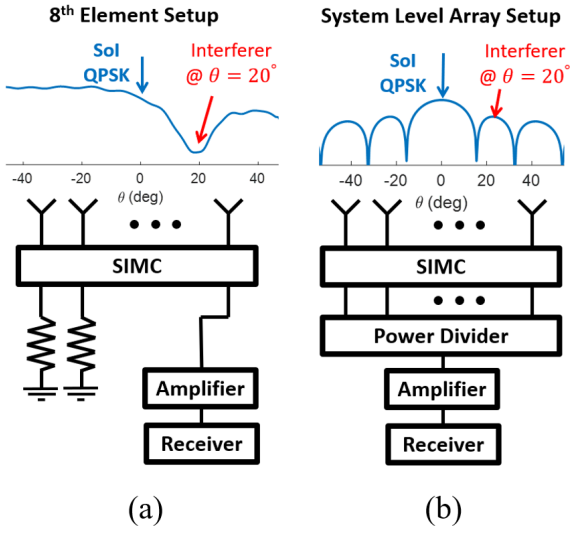

FIGURE 14. Block diagram of the experimental setup where in (a) the nulling is done at an element level, and (b) is done at the array level with the interferer coming in through the first side-lobe.

quadrature hybrids were connected to the phaseshifter boards and the antenna array using coaxial cables. This can be clearly seen in Fig. 11b where it shows the experimental setup placed in the near-field anechoic chamber.

The measured results are compared to the simulated results and shown in Fig. 12 where, as expected, a higher IL due to the unequal power splits is reflected on the embedded element patterns. At best, an IL of 5 dB is achieved; however, deep nulls of more than 15 dB were measured. In both cases, the 7th element was performing better than the 8th, possibly do to the fact that the 8th element is an edge element.

Fig. 10 and Fig. 12 show that there might be some variability in the null placement for the measured results. This highlights the importance of keeping a strict control over the electrical lengths of the cancelling path. The measurements have shown that the best performing element is the 7th because it combines the optimal cancelling signal without being at the edge of the array. Fig. 13 shown the performance of the SIMC's null over all angles of the scanned region of the 7th element. The depth of the null ranges between -20 to -50 dB. A broad range of the depth vs null placement is expected because of the variance in the IL of the phase shifter vs angle.

Together, these results show the ability for the SIMC to place nulls in arbitrary directions, even in finite array cases. To further proof the SIMC, a receiver array is set up and tested with a signal of interest (SoI) while being under stress caused by a strong interferer. This "real case scenario" demonstration is explored in the following section.

IV. 1X8 ARRAY SYSTEM LEVEL DEMONSTRATION

The goal of this research is to reduce the necessary dynamic range of the components in the receiver chain by mitigating

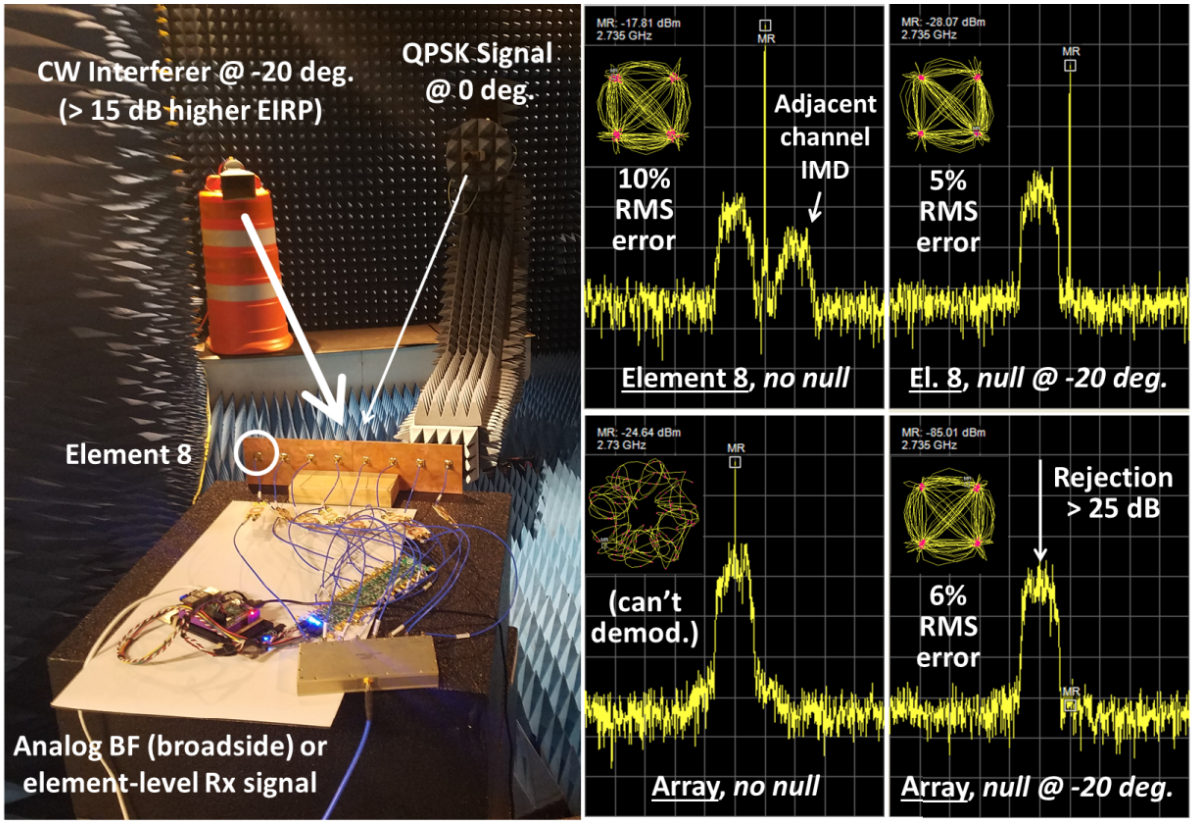

FIGURE 15. (Left) Setup for system-level demonstration of array-level interference rejection; (top right pair) resulting spectra and constellation diagram for a single element, as would be relevant for a digital array, clearly showing effects of IMD and compression; (bottom right pair) corresponding results for an ABF array steered to broadside, with an interferer on top of the signal, showing depth of array-level notch just prior to compression.

potential strong interferers at the RF front-end. In previous sections, the SIMC was demonstrated to work by measuring a null in the embedded element pattern. This section aims to further validate the results of the SIMC and verify that it works when integrated in a typical receiver system. The 1x8 array and the SIMC was connected to an off-the-shelf LNA and a receiver as shown in Fig. 14. Once the system was setup, two signals were transmitted simultaneously and captured by the receiver system.

Both transmitters were set 20° apart from each other. One transmitter was placed at broadside and provided a weak signal of interest (SoI) with a 5 MSPS QPSK signal. The second transmitter provided a strong continuous wave (CW) interference with an incoming angle of −20° off-broadside. Initially, because the null is placed away from the region of interest (at −45° off-broadside) the interferer saturates the LNA and/or the receiver. The goal is to place the null of the SIMC in the direction of the interferer and mitigate it. This would allow the receiver to successfully demodulate the SoI.

The combination of a 1x8 array, the SIMC, the LNA and receiver allowed for two experiments. The first experiment connected the receiver straight to the last antenna element (Element 8) as shown in Fig. 14a, emulating one of the channels of a fully digital array. The other channels were terminated with 50 Ω loads. In this experiment, the CW interferer is set at 2.735 GHz and the SoI at 2.73 GHz. The results of the experiments are shown at the top right pair of Fig. 15, plotted in the frequency domain. At first, the interferer drives the LNA into the non-linear region and creates intermodulation distortion (IMD), raising the SoI's RMS error to 10 %. Then, the null is placed in the direction of the interferer causing the IMD to disappear and reducing the RMS error to 5 %. The reader might observe an interference mitigation of 11 dB as opposed to nulls of more than 15 dB. This effect can be explained as the combination of two factors. The first one is due to the fact that the IL for a specific angle varies for different null placements as seen in Fig. 12. The authors defined the total mitigation as the depth of the null minus the lowest IL of the passband. For the current SIMC configuration, the lowest point of the IL of the passband is 5 dB. When the null is placed far away (−45° 'no-null') the IL of the SIMC at −20° is approximately 9 dB instead of 5 dB, hence reducing the effective mitigation by 4 dB. The second factor is explained by having the LNA operating in the region of strong non-linearities. The interferer is driving the LNA into compression therefore the interferer is less amplified (left of top right pair) then when the LNA is operating in the linear region (right of top right pair).

TABLE 1. Performance summary and comparison to other spatial interference mitigation techniques.

	SNF & FFSNC receiver [16]	Beamforming into LNA [17]	This work, the SIMC
Total null depth	51 dB	$>$ 20 dB	$>$ 20 dB [1]
Noise figure [2]	3.3 dB	6.7 dB	$<$ 1.5 dB [3]
Power handling	LOW	LOW	HIGH
Integration complexity	HIGH	HIGH	LOW
Multiple nulls	YES	NO	NO [4]
Receiver agnostic	NO	YES	YES

[1] Without optimization. [2] At best. [3] Depends on the S_{12a} provided by the two port network. [4] Future investigation

It can be concluded that the total mitigation is similar to the values obtained with the measured embedded element patterns.

The purpose of the second experiment was to to investigate the null itself at the array level so that such effects were ''averaged out''. The system setup was repeated with the difference that all 8 elements were power combined and effectively steered at broadside. The SoI was placed at broadside and the interferer was leaking into the receiver chain through the first sidelobe at $-20°$ as shown in Fig. 14b. To further compromise the integrity of the receiver, the interferer was changed and had the same center frequency as the SoI at 2.73 GHz. This clearly prevented the receiver from demodulating as shown in the bottom pair of Fig. 15. After steering the null in the direction of the interferer, the receiver was able to demodulate the SoI with an RMS of 6 %.

Table 1 summarizes the performance of the other techniques and compares them to the SIMC developed in this work. The SIMC can handle higher power levels provided that the two-port network has a high compression point. This technique is also receiver agnostic, and it is the easiest of the three to be integrated with an arbitrary receiver system. In this work, the depth of the null is not fully optimized and does not correct the amplitude error of the two-port network, resulting in a nulling range from 20 to 50 dB for element 7. The limitation of the null's depth is provided by the calibration and optimization for each nulling angle. As proven in previous sections, the noise figure can be improved by using a tunable two-port network with a reduced IL. Finally, providing multiple nulls for different scan angles is under investigation.

V. CONCLUSION

This paper presents an antenna agnostic spatial interference mitigation circuit. This circuit interconnects antenna elements and creates a steerable null in the embedded element pattern, significantly mitigating the interference at the RF front-end before it enters the receiver. This technique can be used to prevent strong interferers from corrupting the sensitive components in the receiver chain. A complete mathematical model of this circuitry is presented and is proven to accurately predict the behavior of the SIMC in a large array environment. A closed form expression to steer the null at a specified incoming angle is derived. This derivation was expanded to show what can be done to increase the selectivity of the null and to decrease the insertion loss. In order to validate the mathematical model, simulated and experimental results are obtained for a 1x8 array. As a proof of concept, measurements were taken in an anechoic chamber and embedded element patterns with nulls of more than 20 dB were measured. When the array pattern is measured and calculated for a 1x8 array, the performance is decreased because the first element, the one that has no cancellation signal, does not have any spatial mitigation and decreases the performance of the small array. Large arrays, especially the ones that are populated with ''dummy elements'', should not be affected by the performance of the ''first element''. Finally a system-level demonstration with a fully tunable nulling circuitry is provided where an interferer, initially preventing demodulation, was successfully mitigated allowing the receiver to demodulate the signal.

REFERENCES

[1] J. M. Loomis, ''Army radar requirements for the 21st century,'' in *Proc. IEEE Radar Conf.*, Apr. 2007, pp. 1–6.

[2] C. Fulton, P. Clough, V. Pai, and W. Chappell, ''A digital array radar with a hierarchical system architecture,'' in *IEEE MTT-S Int. Microw. Symp. Dig.*, Jun. 2009, pp. 89–92.

[3] N. Peccarelli, B. James, R. Irazoqui, J. Metcalf, C. Fulton, and M. Yeary, ''Survey: Characterization and mitigation of spatial/spectral interferers and transceiver nonlinearities for 5G MIMO systems,'' *IEEE Trans. Microw. Theory Techn.*, vol. 67, no. 7, pp. 2829–2846, Jul. 2019.

[4] S. B. Venkatakrishnan, E. A. Alwan, and J. L. Volakis, ''Wideband RF self-interference cancellation circuit for phased array simultaneous transmit and receive systems,'' *IEEE Access*, vol. 6, pp. 3425–3432, 2018.

[5] M. K. Leino, R. M. Moreno, J. Ala-Laurinaho, R. Valkonen, and V. Viikari, ''Waveguide-based phased array with integrated element-specific electronics for 28 GHz,'' *IEEE Access*, vol. 7, pp. 90045–90054, 2019.

[6] J. G. Andrews, S. Buzzi, W. Choi, S. V. Hanly, A. Lozano, A. C. K. Soong, and J. C. Zhang, ''What will 5G be?'' *IEEE J. Sel. Areas Commun.*, vol. 32, no. 6, pp. 1065–1082, Jun. 2014.

[7] L. Zhang, A. Natarajan, and H. Krishnaswamy, ''Scalable spatial notch suppression in spatio-spectral-filtering MIMO receiver arrays for digital beamforming,'' *IEEE J. Solid-State Circuits*, vol. 51, no. 12, pp. 3152–3166, Dec. 2016.

[8] W. Chappell and C. Fulton, ''Digital array radar panel development,'' in *Proc. IEEE Int. Symp. Phased Array Syst. Technol.*, Oct. 2010, pp. 50–60.

[9] W. Tan, D. Xie, J. Xia, W. Tan, L. Fan, and S. Jin, ''Spectral and energy efficiency of massive MIMO for hybrid architectures based on phase shifters,'' *IEEE Access*, vol. 6, pp. 11751–11759, 2018.

[10] S. H. Talisa, K. W. O'Haver, T. M. Comberiate, M. D. Sharp, and O. F. Somerlock, ''Benefits of digital phased array radars,'' *Proc. IEEE*, vol. 104, no. 3, pp. 530–543, Mar. 2016.

[11] D. C. D. Chang, W. N. Klimczak, and G. C. Busche, ''An experimental digital beamforming array,'' in *Proc. IEEE AP-S. Int. Symp., Antennas Propag.*, vol. 3, Jun. 1988, pp. 1300–1303.

[12] J. H. C. van den Heuvel, J.-P. M. G. Linnartz, P. G. M. Baltus, and D. Cabric, ''Full MIMO spatial filtering approach for dynamic range reduction in wideband cognitive radios,'' *IEEE Trans. Circuits Syst. I, Reg. Papers*, vol. 59, no. 11, pp. 2761–2773, Nov. 2012.

[13] C. Kim, S. Joshi, C. M. Thomas, S. Ha, L. E. Larson, and G. Cauwenberghs, ''A 1.3 mW 48 MHz 4 channel MIMO baseband receiver with 65 dB harmonic rejection and 48.5 dB spatial signal separation,'' *IEEE J. Solid-State Circuits*, vol. 51, no. 4, pp. 832–844, Apr. 2016.

[14] B. James and C. Fulton, "Decorrelation and mitigation of spurious products in phased arrays with direct conversion transceivers," in *IEEE MTT-S Int. Microw. Symp. Dig.*, May 2015, pp. 1–3.
[15] N. Peccarelli and C. Fulton, "Adaptive nonlinear equalization of a tunable bandpass filter," *IEEE Microw. Wireless Compon. Lett.*, vol. 29, no. 2, pp. 149–151, Feb. 2019.
[16] L. Zhang and H. Krishnaswamy, "A 0.1-to-3.1 GHz 4-element MIMO receiver array supporting analog/RF arbitrary spatial filtering," in *IEEE Int. Solid-State Circuits Conf. (ISSCC) Dig. Tech. Papers*, Feb. 2017, pp. 410–412.
[17] S. Jain, Y. Wang, and A. Natarajan, "A 10 GHz CMOS RX frontend with spatial cancellation of co-channel interferers for MIMO/digital beamforming arrays," in *Proc. IEEE Radio Freq. Integr. Circuits Symp.*, May 2016, pp. 99–102.
[18] D. Murphy, H. Darabi, A. Abidi, A. A. Hafez, A. Mirzaei, M. Mikhemar, M.-C. F. Chang, "A blocker-tolerant, noise-cancelling receiver suitable for wideband wireless applications," *IEEE J. Solid-State Circuits*, vol. 47, no. 12, pp. 2943–2963, Dec. 2012.
[19] R. Irazoqui and C. Fulton, "Spatial interference mitigation nulling the embedded element pattern," in *IEEE MTT-S Int. Microw. Symp. Dig.*, Jun. 2018, pp. 620–623.
[20] N. Peccarelli, R. Irazoqui, and C. Fulton, "Mitigation of interferers and nonlinear spurious products for digital array and MIMO systems," in *IEEE MTT-S Int. Microw. Symp. Dig.*, Jun. 2019, pp. 1233–1236.
[21] A. K. Bhattacharyya, *Phased Array Antennas: Floquet Analysis, Synthesis, BFNs and Active Array Systems*. Hoboken, NJ, USA: Wiley, 2006.
[22] E. Holzman, "On the use of dummy elements to match edge elements in transmit arrays," in *Proc. Int. Symp. Phased Array Syst. Technol.*, Oct. 2013, pp. 549–552.

ROBIN W. IRAZOQUI received the B.S. degree in industrial engineering from the Universitat de Girona, Girona, Spain, in 2012, and the M.S. and Ph.D. degrees in electrical and computer engineering from the Advanced Radar Research Center, The University of Oklahoma, in 2014 and 2019, respectively. His research interests include RF component design, RF front-end designs, and system level integration with an emphasis on digital arrays.

CALEB J. FULTON (S'05–M'11–SM'16) received the B.S. and Ph.D. degrees in ECE from Purdue University, West Lafayette, IN, USA, in 2006 and 2011, respectively. He is currently an Assistant Professor in ECE with the Advanced Radar Research Center, The University of Oklahoma, Norman, OK, USA. His research interests include antenna design, digital phased array calibration and compensation for transceiver errors, calibration for high-quality polarimetric radar measurements, integration of low-complexity transceivers and high-power GaN devices, and advanced digital beamforming design considerations. He is also involved in a number of digital phased array research and development efforts for a variety of applications. He is a member of the IEEE Antennas and Propagation, Aerospace and Electronic Systems, and Microwave Theory and Techniques Societies, and serves on the Education Committee of the latter. He was a recipient of the Purdue University Eaton Alumni Award for Design Excellence for his work on the Army Digital Array Radar (DAR) Project, in 2009. He was also a recipient of the Meritorious Paper Award for a summary of these efforts at the 2010 Government Microcircuit Applications and Critical Technologies Conference and the 2015 DARPA Young Faculty Award for his ongoing digital phased array research.